IEEE Access
Multidisciplinary ⋮ Rapid Review ⋮ Open Access Journal

Received November 15, 2019, accepted December 7, 2019, date of publication December 27, 2019,
date of current version January 22, 2020.

Digital Object Identifier 10.1109/ACCESS.2019.2960563

Improvements to Terrain Aided Navigation Accuracy in Deep-Sea Space by High Precision Particle Filter initialization

WANG RUPENG[1], LI YE[2], MA TENG[2], CONG ZHENG[2], GONG YUSEN[2], AND XU PENGFEI[1]

[1]Key Laboratory of Coastal Disaster and Defence, Ministry of Education, Hohai University, Nanjing 210098, China
[2]Science and Technology on Underwater Vehicles Laboratory, Harbin Engineering University, Harbin 150001, China

Corresponding author: Li Ye (liyeheu103@163.com)

This work was supported in part by the National Key Research and Development Plan under Grant 2017YFC0305700, in part by the Marine Science and Technology Innovation Project of Jiangsu Province under Grant hy2018-15, in part by the National Natural Science Foundation of China under Grant 51909245, and in part by the Open Fund of Key Laboratory of High Performance Ship Technology (Wuhan University of Technology), Ministry of Education, under Grant gxnc19051802.

ABSTRACT AUV (autonomous underwater vehicles) are required to have long-term and high-precision positioning capability relative to seabed targets in most deep-sea exploration tasks. However, acoustic positioning error is positively correlated with its operating range and inertial navigation has inevitable accumulated time errors, neither of which provide precise AUV positions. TAN (terrain aided navigation) directly calculates the AUV position to the seabed terrain coordinate system by tracking the seabed topographic characteristics, which can guide the AUV to seabed target accurately. However, the initial TAN positioning error will increase with the AUV operation depth, which causes a large PF (particle filter) initialization error and particle coverage interval, and will affect the convergence and stability of TAN. To solve this problem, we first propose a TAP (terrain aided position) confidence interval model. We then use the confidence interval to constrain the initial particles to a smaller range. Finally, the validity of the algorithm is verified by playback simulation with ship-borne multi-beam sonar sensor measured data. The results show that the TAP confidence interval can reduce the coverage of the initial particle, and can improve the convergence speed and filtering accuracy of the TAN.

INDEX TERMS Autonomous underwater vehicle, terrain-aided navigation, particle-filter, underwater navigation, confidence interval.

I. INTRODUCTION

Seabed space, especially deep seabed space, contains abundant resources closely related to the future development of mankind. Many countries are devoting themselves to exploring and exploiting seabed space. To this end, many underwater vehicles have been developed for exploring deep seabed. High-precision navigation information is the basis for the safe and stable operation of deep-sea underwater robots and is the basic information needed for AUV (autonomous underwater vehicles) to perform ocean exploration tasks. In situ observations and sampling of seabed environmental information, the fixed-point operation of a seabed target area, and the fine detection and salvage of seabed targets requires underwater vehicles to have the ability to accurately locate seabed target points. As shown in Fig.1, acoustic positioning errors increase with distance and the DR (Dead reckoning) position includes inevitable cumulative error, which makes the AUV positioning in deep seabed space have larger uncertain intervals. This results in AUV being unable to accurately arrive at the target point in the seabed. Therefore, there is an urgent need for an accurate position method without cumulative errors and distance correlation errors in order to accurately guide AUV to reach the target point in the seabed topographic space.

TAN (Terrain aided navigation) positioning AUV are used to track seabed terrain features in seabed space. It can provide bounded error positions for AUV in infinite time. As shown in Fig.2a. TAN is a kind of integrated navigation method, which includes a reference navigation system and a terrain

The associate editor coordinating the review of this manuscript and approving it for publication was Haluk Eren.

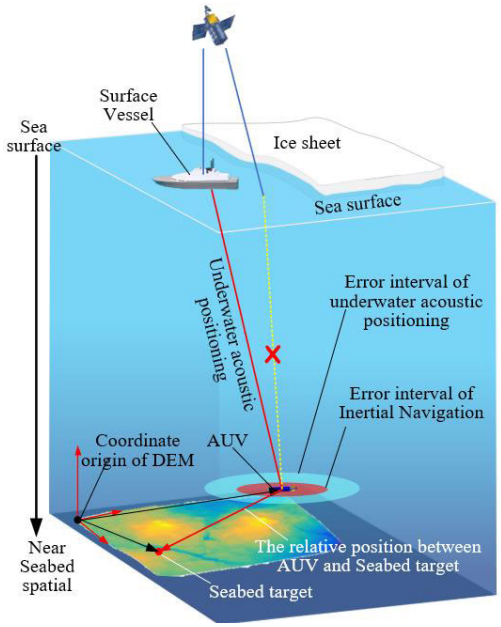

FIGURE 1. Inaccuracies in commonly used positioning methods in seabed space.

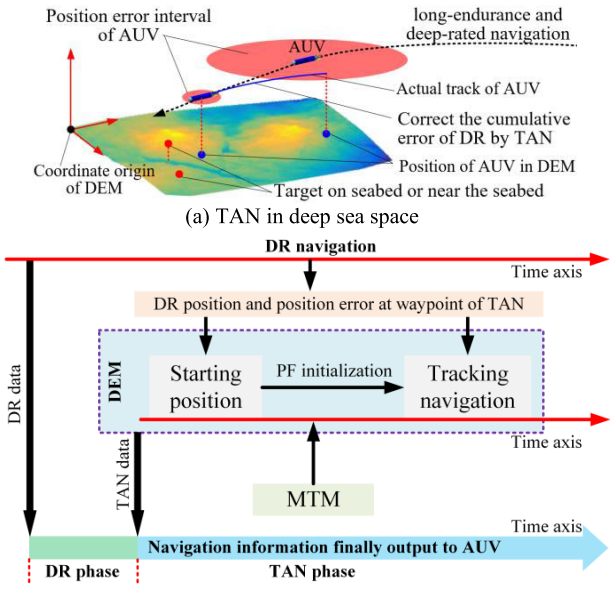

FIGURE 2. Using terrain-guided AUV for seabed target location.

matching positioning unit. The reference navigation system is usually integral navigation mode, such as DR [9], [25]. Due to the time accumulation error of DR Navigation, and the error of terrain matching positioning is bounded, the terrain matching positioning can constrain the accumulation of Dr error, and the correlation of DR Navigation can constrain the skip point phenomenon of terrain matching positioning. The terrain matching navigation system uses fusion algorithm to fuse two kinds of navigation information online, so as to improve the positioning accuracy. Due to the time accumulation error of DR Navigation, and the error of terrain matching positioning is bounded, the terrain matching positioning can constrain the accumulation of DR error, and the correlation of DR Navigation can constrain the skip point phenomenon of terrain matching positioning. The terrain matching navigation system uses fusion algorithm to fuse two kinds of navigation information online. In the seabed area without prior topographic map, AUV uses pure DR Navigation for positioning. After entering the prior topographic map area and starting the terrain matching navigation system. Then, the system measures the seabed terrain under AUV in real time and carries out online matching positioning with prior topographic map and estimates the location of AUV iteratively through filtering algorithm (Fig.b). Because the location error of TAP is bounded, it can constrain the error accumulation of DR. TAN solves for the AUV position in the topographic map coordinate system, so it can guide it to the seabed target accurately.

The state transition equation of TAN system is shown in equation (1), and the state $\boldsymbol{X}_t$ is given by the DR system [23].

$$\begin{cases} \boldsymbol{X}_{t+1} = \boldsymbol{X}_t + \boldsymbol{u}_t + \boldsymbol{v}_t \\ \boldsymbol{Z}_t = h\left(\boldsymbol{X}_t\right) + \boldsymbol{E}_t \\ t = 0, 1, 2, 3 \ldots \end{cases} \tag{1}$$

where $\boldsymbol{X}_{t+1}$, $\boldsymbol{X}_t$ are the position in the horizontal plane at time t and $t+1$ respectively; $\boldsymbol{u}_t$ represent the travel distance between t and $t+1$ and it is provided by the DR system. The measured depths to the bottom are collected in the matrix $\boldsymbol{Z}_t$ and the matrix $h\left(\boldsymbol{X}_t\right)$ collects the depths according to the map if AUV is in position $\boldsymbol{X}_t$. The error in the DR system is $\boldsymbol{v}_t$, where $\boldsymbol{v}_t$ is an additive white noise input. In TAN system, $\boldsymbol{u}_t$ and $\boldsymbol{v}_t$ are directly given by DR. $\boldsymbol{E}_t$ is the error in the depth measurement at time t, the variance estimates are described in equation (2).

At present, TAN based research on seabed topographic mapping, seabed environmental information in situ observation and space-time synchronous modeling [2]–[4], AUV ultra-long range high-precision navigation [5], [6], etc. has been carried out. TAN has become a new navigation technology aimed at use for near seabed space.

II. RELATED WORKS

TAN includes two stages: initial positioning and tracking filtering [7]. The purpose of the initial phase is to reduce the positioning deviation of the starting point, to ensure that the TAN system can converge steadily and track to the correct position in the tracking filtering stage as shown in Fig.3. In the past 20 years, underwater TAN research has been focused on tracking filtering methods, such as PF (particle filter) [8]–[10], robust PF [11]–[13], and PMF (point mass filter) [14]–[18]. The PF method is the best filter method for TAN systems because of its advantages in dealing with the state estimation of non-linear and non-Gaussian systems [19].

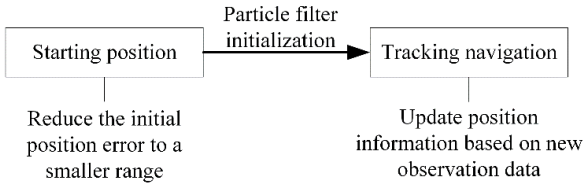

FIGURE 3. **The two TAN phases and their tasks.**

The tracking navigation filtering TAN theory is not new, but research on initial positioning is rare.

In [7], the TERCOM (terrain contour matching) algorithm was proposed to estimate the initial position; however, the probability of pseudo-peaks and mismatches increased with the increase in the initial search area, making the positioning results very unstable. Reference [20] addressed the initial positioning problem for aircraft TAN, by proposing the use of continuous acquisition of many TERCOM points, where the consistency of these TERCOM points was tested. The points that pass the consistency test can be identified as initial positions, as used by reference [21] for underwater geomagnetic navigation. This method needs a wide range of suitable matching areas and is not suitable for the initial position of underwater TAN. Similar problems are mentioned in [22], which proposed an effectiveness testing method and recovery method for the TAP (terrain-aided positioning) system in case of large abrupt position deviation; however, there is no in-depth study on the reinitialization after the generation of large bias. In [7], the author divides underwater TAN into two phases, the initial phase and the tracking phase. The task of the initial phase is to reduce the cumulative error of the reference navigation to a smaller range using the matching positioning method, and then the tracking phase, which estimates the location of AUV recursively by filter. The stability and positioning accuracy in the initial TAN stage cannot be ignored, especially in the case of large initial positioning deviations.

In order to verify the possibility of correcting the AUV accumulated error using TAN technology we wanted to test AUVs deployed by deep diving and ultra-long cruises (Fig.4a). We carried out an experiment in August 2017 in the Zhongsha Reef Sea Area, Jiaozhou Bay, Shandong Province (Fig.4b). However, our filter, unfortunately, did not converge to the correct position.

As shown in Fig.5a, the accumulated error caused the DR position probability distribution of the initial TAN waypoint to significantly deviate from reality. There are also pseudo-peaks and pseudo-positioning points in the probability distribution of the TAP of the initial TAN waypoint (Fig.5b). As shown in Fig.6, the initial particle distribution is obtained by sampling from the probability distribution position of the initial TAN waypoint, where each particle has a position parameter and a weight parameter to represent the probability of the particle location. However, the initial positioning probability distribution function has been seriously distorted, which will lead to a large coverage of the initial particle and the particles distribution having a serious deviation from the true value.

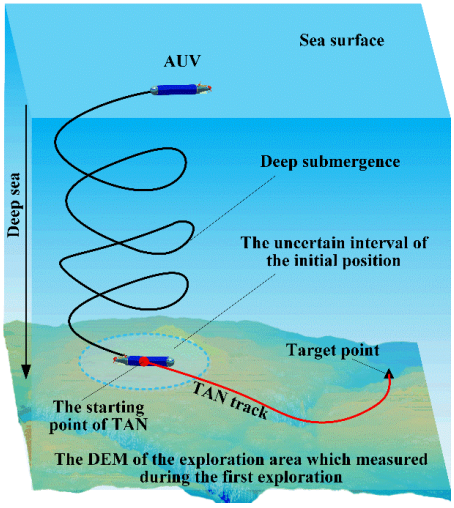

(a) AUV corrects TAN errors after large diving depths and ultra-long-range missions

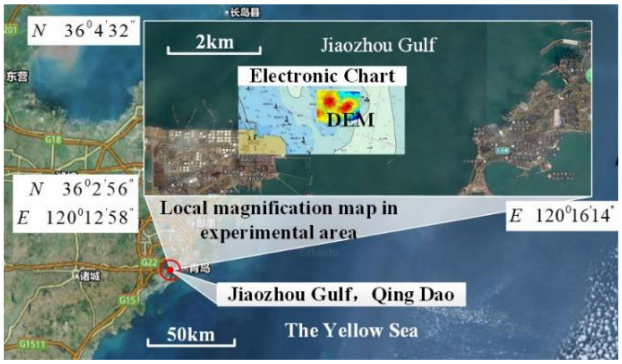

(b) Geographical location of the experimental area

FIGURE 4. **Experiment area and experiment simulation scenario.**

As shown in Fig.7a, if the PF cannot converge quickly in the initial stage, it will very likely diverge once the AUV enters the low matching adaptability area (Fig.7b). The initialization accuracy and coverage of the initialization particle will directly affect the stability and accuracy of TAN. The high-precision PF initialization is crucial, especially when the initial position error is large. Therefore, the PF TAN initialization must be paid attention to.

This study proposes using the PF initialization by using the confidence interval of TAP, such that the initial particle approximates the real position. The main purpose of this study is to solve the PF initial positioning problem when the TAN initial positioning system error is large, and to ensure the fast convergence of the initial particle approximation to the real position and initial stage. The rest of the paper mainly includes: **Section II**:confidence interval estimation method based on the TAP position jump model is introduced; **Section III:** PF initialization based on the effective position points of TAP is discussed along with two types of initial weight distribution methods, and the TAN accuracy and

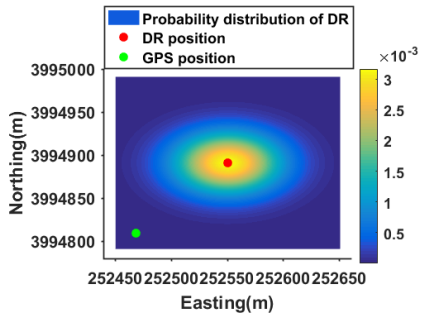

(a) DR position and its probability distribution

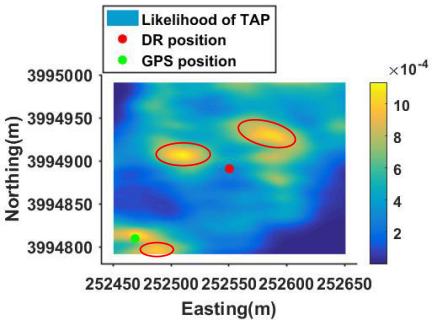

(b) TAP position and its probability distribution

FIGURE 5. The cloud chart of position probability distribution.

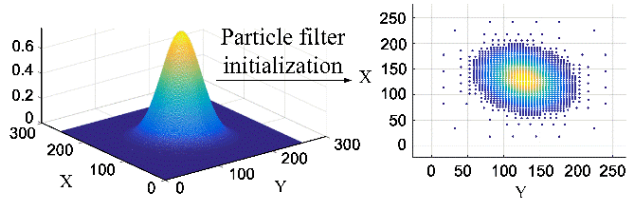

FIGURE 6. Schematic diagram of particle filter initialization.

stability with initialization method based on effective TAP is compared with the other two particle-filter initialization methods. **Section V**: shows the conclusion.

III. TAP CONFIDENCE INTERVAL

At present, there are two ways to estimate the TAP confidence interval. The first is to replace the confidence interval boundary with the CRLB (Cramer-Rao Lower Bound) [7]. However, the CRLB needs to be computed at a known TAP position, and it cannot handle issues such as multiple pseudo-peaks and pseudo-positions. As shown in Fig.8a, the self-similarity of the terrain results in multiple pseudo-peaks in the searching area, and the CRLB of each peak is different. In this case, it is impossible to obtain an accurate confidence interval. Fig.8b shows the mismatch, mainly caused by local topographic distortion. The peak at the mismatched position is clearly higher and sharper than that near the true position, which will produce a wrong CRLB. Fig.8c shows the anisotropy of TAP. It can be seen that the probability distribution is different in different directions, and the anisotropy TAP character cannot be accurately described by the CRLB.

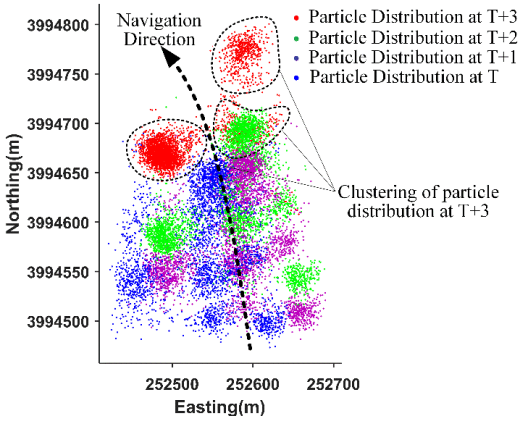

(a) Multi-center particle clustering

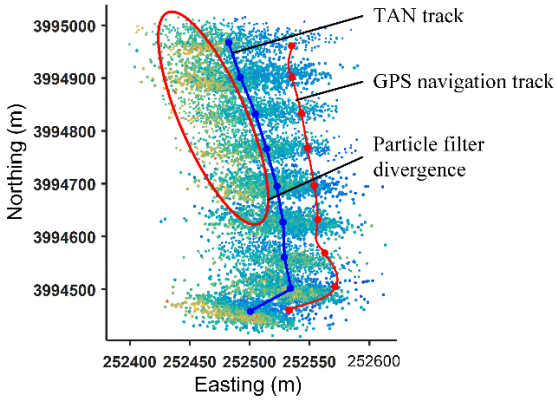

(b) Filtering divergence in low adaptability areas

FIGURE 7. Large initial particle coverage interval and low terrain adaptability causes filter divergence.

The other is hypothesis test method based on statistics of terrain matching residuals [23]. Assuming there are m × n terrain nodes in MTM. In fact, this method regards the measurement error of a terrain node as Gauss distribution, and then the measurement error of MTM obeys the chi-square distribution of degree of freedom (mn − 1). It didn't consider the nonlinear mapping relations $\boldsymbol{Z} = h(\boldsymbol{X}^p) + \boldsymbol{E}$ between measured terrain $\boldsymbol{Z}$ and the TAP $\boldsymbol{X}^p$. $h(.)$ represents the equation of terrain surface. which is an unknown mapping relationship and has strong nonlinearity, $\boldsymbol{E}$ is the error in the depth measurement (possibly including map errors, tide level, interpolation errors etc.).

Based on the above reality, this study is the first to propose a confidence interval estimation method based on the TAP position jump model. As shown in Fig.9, the black and gray points represent the searching points, and the ellipse represents the contour of the likelihood function. The peak of likelihood function (red point) is obtained by Equation (2).

$$\boldsymbol{X}^p = \underset{\boldsymbol{X}^{kl} \in X^s}{\operatorname{argmax}} \left\{ \mathrm{C} \cdot \exp\left(- \frac{\sum_{i=1}^{\mathrm{m}} \sum_{j=1}^{\mathrm{n}} \left(h_{ij}\left(\boldsymbol{X}^{kl}\right) - z_{ij} - t^{kl} \right)}{2\mathrm{mn}\left(\sigma^{kl}\right)^2} \right) \right\} \tag{2}$$

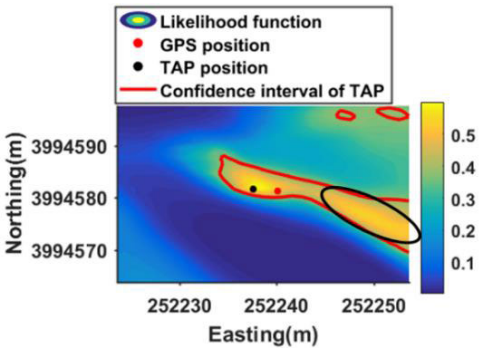

(a) TAP likelihood has pseudo-peaks (in black oval).

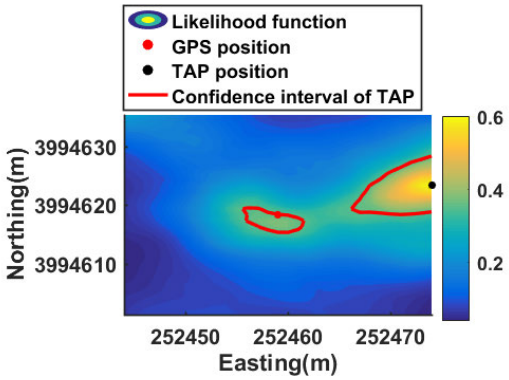

(b) Pseudo-position in TAP likelihood function

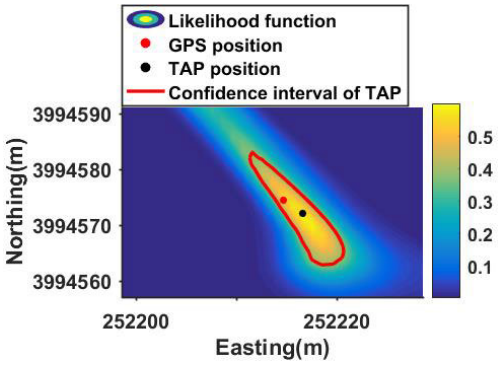

(c) Anisotropy characteristics of TAP

Fig.8 Several typical TAP likelihood functions

FIGURE 8. Several typical TAP likelihood functions.

where $\boldsymbol{X}^p$ represents the TAP point; X^s represents a search interval, $\boldsymbol{X}^p \in \left\{\boldsymbol{X}^{kl}, k = 1, 2, 3 \ldots \mathrm{m}, l = 1, 2, 3 \ldots \mathrm{n}\right\}$, and m, n represent the rows and columns of the search point set, $\boldsymbol{X}^p \in X^s$, $\boldsymbol{X}^{kl} \in X^s$; $h_{ij}\left(\boldsymbol{X}^{kl}\right)$ refers to the interpolation elevation value whose index is ij in the interpolation elevation sequence of $\boldsymbol{X}^{kl}$ position in the prior topographic map; t^{kl} refers to the tidal range value of the search point whose index number is kl; z_{ij} refers to the height value whose index number is ij in the measurement topographic elevation sequence.

Based on the likelihood function of the vertical section through the TAP position (Fig.9), because of position uncertainty, the TAP position will tend to jump to other searching points with a certain probability. With the decrease in the likelihood function of one searching point, the probability of the TAP jumping to that point will decrease. Until the

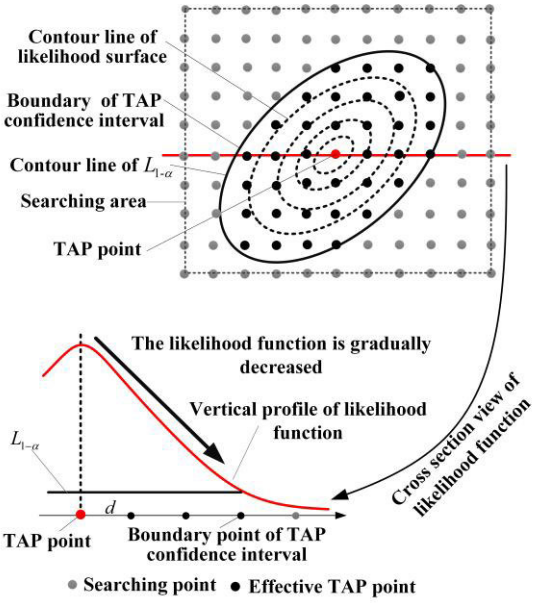

FIGURE 9. Map of the TAP point confidence intervals and boundary points.

likelihood function drops to a certain value $L_{1-\alpha}$, the TAP point will jump to it with a very small probability, α. This point is defined as the boundary point of the confidence interval of the TAP likelihood function, with a confidence level of $1-\alpha$.

Positioning deviation is mainly caused by TAN sensor measurement error and terrain interpolation error. It is difficult to obtain the relationship between terrain measurement errors and TAN sensor errors, because of the coupling effect between the TAN sensor errors; however, it can be estimated by matching residuals, according to the conclusions of [7]. Thus, the residual of the multi-beam TAP has the characteristics of a progressive Gaussian distribution, and the residuals can be assumed to obey the Gaussian distribution when the position estimation is carried out. Suppose we get the TAP position $\boldsymbol{X}^p$, the MTM sequence is z_{ij}, and the interpolation sequence of MTM in a DEM at the TAP position is $h_{ij}(\boldsymbol{X}^p)$. Assume the height residual sequence $\Delta h_{ij}(\boldsymbol{X}^p)$ represents the difference between $h_{ij}(\boldsymbol{X}^p)$ and z_{ij}, and $\Delta h_{ij}(\boldsymbol{X}^p)$ can be regarded as the observation sequence of terrain elevation measurement error $\boldsymbol{E} \sim N(t^p, \sigma^p)$. Tidal t^p and measurement error standard deviation σ^p at the TAP position can be obtained according to Equation (3):

$$\begin{cases} \Delta h_{ij}(\boldsymbol{X}^p) = h_{ij}(\boldsymbol{X}^p) - z_{ij} \\ t^p = \dfrac{1}{\mathrm{mn}} \sum\limits_{i=1}^{\mathrm{m}} \sum\limits_{j=1}^{\mathrm{n}} \Delta h_{ij}\left(\boldsymbol{X}^p\right) \\ S^p = \sqrt{\dfrac{\sum\limits_{i=1}^{m} \sum\limits_{j=1}^{n} \left(\Delta h_{ij}\left(\boldsymbol{X}^p\right) - t^p\right)^2}{\mathrm{mn} - 1}} \\ \sigma \approx \lambda \cdot S^p \end{cases} \tag{3}$$

where it represents the interpolation height sequence of MTM at $\boldsymbol{X}^p$ in DEM (Digital Elevation Map), S^p represents the

estimation of the standard deviation of the measurement error, and λ is the correction parameter that considers the non-Gaussian distribution of the residuals.

According to the conclusions of [7], in the case of sufficient measurement data, the TAP residual is the asymptotic Gaussian distribution. The following two assumptions can be obtained:

Assumption 1: *The height residual sequence $\Delta h(\boldsymbol{X}^p)$ at the TAP point obeys the Gaussian distribution* $\mathrm{N}\left(0, \left((\sigma^p)^2\right)\right)$;

Assumption 2: *The measurement error of each measuring point $\Delta h_{ij}(\boldsymbol{X}^p)$ obeys the same distribution* $\mathrm{N}\left(0, \left((\sigma^p)^2\right)\right)$.

Equation (3) yields the tide and measurement error estimates at the TAP position, and substitutes them into Equation (1). Using the logarithmic form of Equation (1), it can be written as (4):

$$l\left(\boldsymbol{X}^p\right) = ln\left(\mathrm{C}\right) - \frac{1}{2\mathrm{mn}} \sum_{i=1}^{\mathrm{m}} \sum_{j=1}^{\mathrm{n}} \frac{\left(h_{ij}\left(\boldsymbol{X}^p\right) - z_{ij} - t^p\right)^2}{(\sigma^p)^2} \tag{4}$$

This assumes the likelihood surface represents a biquadric surface in the confidence interval of $\boldsymbol{X}^p$. Any $\boldsymbol{X}$ in the confidence interval of X^p can be rewritten into the quadratic shape function form $l\left(\boldsymbol{X}\right)$:

$$l\left(\boldsymbol{X}\right) = ln\left(\boldsymbol{X}^p\right) + \frac{1}{2}\frac{\partial^2 l\left(\boldsymbol{X}^p\right)}{\partial \boldsymbol{e}^2}\left|\Delta \boldsymbol{x_e}\right|^2 + 0\left(\left|\Delta \boldsymbol{x}\right|^n\right) \tag{5}$$

where $\Delta \boldsymbol{x_e}$ represents the position deviation $\Delta \boldsymbol{x_e} = \boldsymbol{X}^p - \boldsymbol{X}$, $\boldsymbol{e}$ represents the unit direction vector of $\Delta \boldsymbol{x_e}$, and $0\left(\left|\Delta \boldsymbol{x_e}\right|^n\right)$ represents the higher order infinitesimal of $\Delta \boldsymbol{x_e}$.

The residuals square sum function of the TAP position can be defined by Equation (6):

$$\begin{cases} S\left(\boldsymbol{X}^p\right) = \sum_{i=1}^{\mathrm{m}} \sum_{j=1}^{\mathrm{n}} \left(h_{ij}\left(\boldsymbol{X}^p\right) - z_{ij} - t^p\right)^2 \\ S_{ij}\left(\boldsymbol{X}^p\right) = \left(h_{ij}\left(\boldsymbol{X}^p - z_{ij} - t^p\right)\right)^2 \end{cases} \tag{6}$$

In the same way, this assumes the likelihood surface represents a biquadric surface in the confidence interval of $\boldsymbol{X}^p$. Any $\boldsymbol{X}$ in the confidence interval of $\boldsymbol{X}^p$ can be rewritten into the quadratic shape function form $S\left(\boldsymbol{X}\right)$:

$$S\left(\boldsymbol{X}\right) = S\left(\boldsymbol{X}^p\right) + \frac{\partial S\left(\boldsymbol{X}^p\right)}{\partial \boldsymbol{e}}\Delta \boldsymbol{x_e} + \frac{1}{2}\frac{\partial^2 S\left(\boldsymbol{X}^p\right)}{\partial \boldsymbol{e}^2}\left|\Delta \boldsymbol{x_e}\right|^2 + 0\left(\left|\Delta \boldsymbol{x_e}\right|^n\right) \tag{7}$$

where, $\boldsymbol{e} = \left(\boldsymbol{e_x}, \boldsymbol{e_y}\right)$ represent unit direction vector; Because $\frac{\partial S(\boldsymbol{X}^p)}{\partial \boldsymbol{e}}$ is equal to zero at the TAP position, (7) can be simplified to (8):

$$S\left(\boldsymbol{X}\right) \approx S\left(\boldsymbol{X}^p\right) + \frac{1}{2}\frac{\partial^2 S\left(\boldsymbol{X}^p\right)}{\partial \boldsymbol{e}^2}\left|\Delta \boldsymbol{x_e}\right|^2 \tag{8}$$

where $S\left(\boldsymbol{X}\right)$ represents the residual sum of the squares function at the real AUV location and $S\left(\boldsymbol{X}^p\right)$ represents the residual sum of the squares function at the TAP position. According to the theory of parameter estimation, we obtained the information matrix for the TAP position using (9):

$$I = \frac{1}{2\left(\sigma^p\right)^2}\mathrm{E}\left(\frac{\partial^2 S\left(\boldsymbol{X}^p\right)}{\partial \boldsymbol{e}^2}\right) \tag{9}$$

According to the previous hypothesis, $S\left(\boldsymbol{X}^p\right)$ is an approximate quadratic shape function form at $\boldsymbol{X}^p$. According to the statistical theory of parameter estimation, the variance $E\left(\left|\Delta \boldsymbol{x_e}\right|^2\right)$ of the estimated value, $\boldsymbol{X}^p$, can be obtained by the information matrix using Equation (10).

$$E\left(\left|\Delta \boldsymbol{x_e}\right|^2\right) = I^{-1} = 2\left(\sigma^p\right)^2\left[\mathrm{E}\left(\frac{\partial^2 S\left(\boldsymbol{X}^p\right)}{\partial \boldsymbol{e}^2}\right)\right]^{-1} \tag{10}$$

Assuming the dimensions of MTM are mn, according to the premise in **Section 2**, the terrain nodes measurement error is independent and identically distributed $\mathrm{N}\left(0, \left(\sigma^p\right)^2\right)$. According to the conclusions in [24], for a given σ^p, if $l\left(\boldsymbol{X}^p\right)$ is an approximate quadratic surface about parameter, $\boldsymbol{X}$, near the TAP position, $\boldsymbol{X}^p$, a confident interval that is more than confidence $1-\alpha$ can be defined as (11).

$$\frac{\partial^2 l\left(\boldsymbol{X}^p\right)}{\partial \boldsymbol{e}^2}\left|\Delta \boldsymbol{x_e}\right|^2 < \chi^2_{1-\alpha}\left(\mathrm{mn}-1\right) \tag{11}$$

Based on Equations (4) and (6), Equation (12) can be obtained.

$$\frac{\partial^2 l\left(\boldsymbol{X}^p\right)}{\partial \boldsymbol{e}^2} \approx \sum_{i=1}^{\mathrm{m}} \sum_{j=1}^{\mathrm{n}} \frac{1}{2\left(\sigma^p\right)^2}\frac{\partial^2 S_{ij}\left(\boldsymbol{X}^p\right)}{\partial \boldsymbol{e}^2} \tag{12}$$

Then, we can obtain Equation (13) according to Inequality (11) and Equation (12).

$$\sum_{i=1}^{\mathrm{m}} \sum_{j=1}^{\mathrm{n}} \frac{1}{2\left(\sigma^p\right)^2}\frac{\partial^2 S_{ij}\left(\boldsymbol{X}^p\right)}{\partial \boldsymbol{e}^2}\left|\Delta \boldsymbol{x_e}\right|^2 < 2\left(\sigma^p\right)^2\chi^2_{1-\alpha}\left(\mathrm{mn}-1\right) \tag{13}$$

According to Equation (3), the following equation is established:

$$2\left(\sigma^p\right)^2 = \frac{\lambda}{\mathrm{mn}-1}S\left(\boldsymbol{X}^p\right) \tag{14}$$

By introducing the form of (14) into (7), we can obtain the $1-\alpha$ confidence interval isoline of the square sum function of the TAP (15):

$$S\left(\boldsymbol{X}\right)_{1-\alpha} \approx S\left(\boldsymbol{X}^p\right)\left[1 + \lambda\frac{\chi^2_{1-\alpha}\left(\mathrm{mn}-1\right)}{\mathrm{mn}-1}\right] \tag{15}$$

By introducing (15) into Equation (3), the $1-\alpha$ confidence interval isoline of the likelihood function of TAP can be established:

$$L_{1-\alpha} = \mathrm{C}\cdot\exp\left(-\frac{S\left(\boldsymbol{X}\right)_{1-\alpha}}{\left(\sigma^p\right)^2}\right) \tag{16}$$

The new TAP confidence interval estimation method mentioned in this paper considers the biquadric surface character of the TAP likelihood function and has higher accuracy. The amplification coefficient, λ, is usually chosen in the interval $\lambda > 1$, because of the terrain measurement error is not absolutely Gaussian white noise. Fig.10a shows the DR track, GPS track of the experiment route, and DR position confidence interval and searching area of each waypoint. Fig. 10b shows the estimate result using the new method.

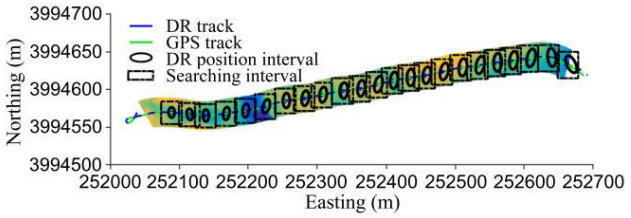

(a) Measurement data and search interval of TAP

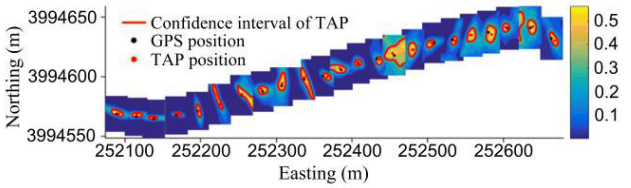

(b) TAP likelihood function and TAP confidence interval

FIGURE 10. Likelihood function and confidence interval of the TAP based on the new algorithm ($\lambda = 1$).

The Monte Carlo method is used to simulate and verify the positioning. A total of 1000 positioning experiments were carried out. In the experiment, N (0, 0.2) Gauss noise is added to the measured terrain. A total of 7050 TAP positioning points that include false points and mismatched points, marked as color dots in Fig.11, were obtained. The TAP confidence interval is 95%, and the red solid line in Fig.11 is the edge of TAP confidence interval. There are 157 points outside the confidence interval, and the effective point ratio is 2.23%.

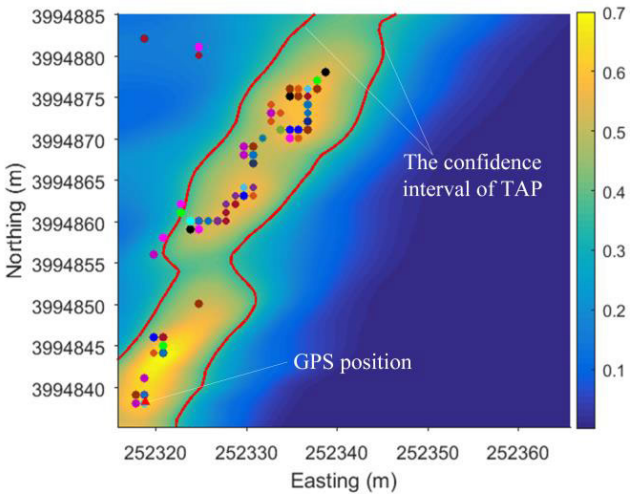

FIGURE 11. Monte Carlo simulation results of TAP.

IV. PARTICLE INITIALIZATION IN THE INITIAL TAN STAGE

The PF initialization with effective TAP includes two parts: initial TAP and likelihood function refinement, and calculation of effective TAP position and distributed particle. Let us assume that in the initial TAN time the cumulative error of

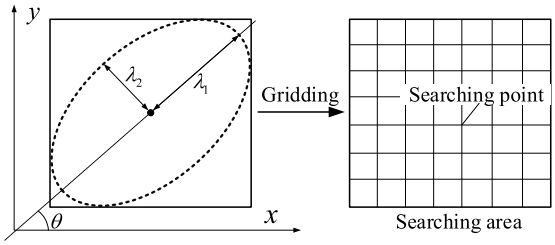

FIGURE 12. Diagram of search interval computation.

DR is $\boldsymbol{P}_0$.

$$\boldsymbol{P}_0 = \begin{bmatrix} \sigma_x^2 & \sigma_{xy} \\ \sigma_{yx} & \sigma_y^2 \end{bmatrix} \tag{17}$$

where $\boldsymbol{P}_0$ represents the DR error at the first waypoint in the initial phase of TAN; σ_x and σ_y represent the error in the x and y directions, respectively; and σ_{xy} is the covariance of the DR navigation error in the x and y directions.

Fig.12 shows the elliptical DR position confidence interval. The minimum rectangular interval containing the confidence interval can then be calculated and it is called the TAP searching area [23]. The calculation methods of parameters of $\lambda_1, \lambda_2, \theta$ are as follows (18). Finally, the continuous search interval is discretized using a gridding method.

$$\begin{cases} \lambda_1 = \dfrac{1}{2}\left[\sigma_x^2 + \sigma_y^2 + \sqrt{\left(\sigma_x^2 - \sigma_y^2\right) + 4\sigma_{xy}^2}\right] \\ \lambda_2 = \dfrac{1}{2}\left[\sigma_x^2 + \sigma_y^2 - \sqrt{\left(\sigma_x^2 - \sigma_y^2\right) + 4\sigma_{xy}^2}\right] \\ \theta = \dfrac{1}{2}\arctan\left(\dfrac{2\sigma_{xy}}{\sigma_x^2 - \sigma_y^2}\right) \end{cases} \tag{18}$$

A. INITIAL TAP AND LIKELIHOOD FUNCTION REFINEMENT

The probability distribution function of the terrain matching location is obtained by calculating the similarity between the measured terrain and priori terrain. The similarity between the measured terrain and priori terrain correspond to search points and reflects the probability that AUV is located at that point at the moment (Fig.13). As can be seen from the schematic diagram, the search point is actually the grid node in the search area, so the time consumed in the matching process is related to the grid scale of the search area. The smaller the scale, the greater the time consumed.

A larger searching step is used to improve computing speed. Then, the likelihood function mesh is refined by the interpolation algorithm. Fig.14a and b shows the likelihood function with a 4 m searching step which is then interpolated into 1 m × 1 m. Fig.15 shows the time consumption and interpolation error while the searching step is 1 m, 2 m, 3 m, and 4 m, then interpolated into the 1 m × 1 m. The time consumption decreases rapidly with an increase in the searching step size. The interpolation error is small at the 3 m searching

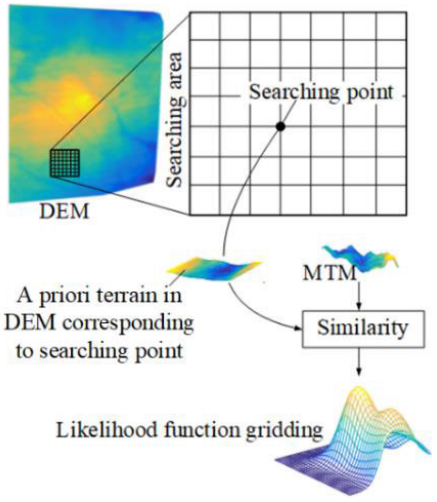

FIGURE 13. Diagram of computing TAP likelihood function.

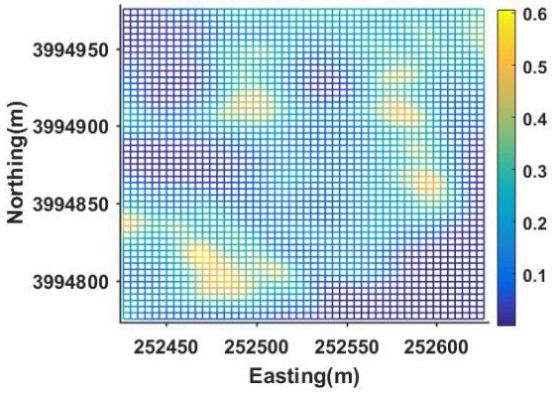

(a) TAP likelihood with mesh size 4 m × 4 m

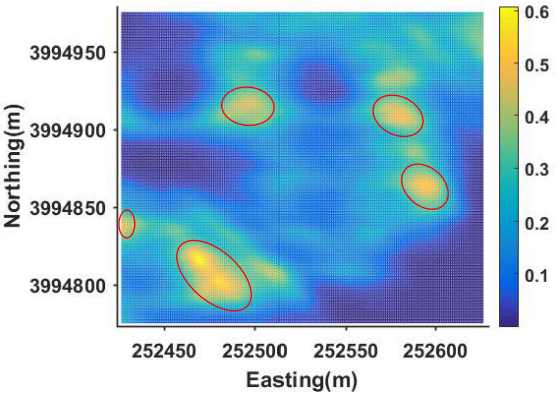

(b) Interpolated likelihood with mesh size 1 m × 1 m

FIGURE 14. Mesh refinement by interpolation.

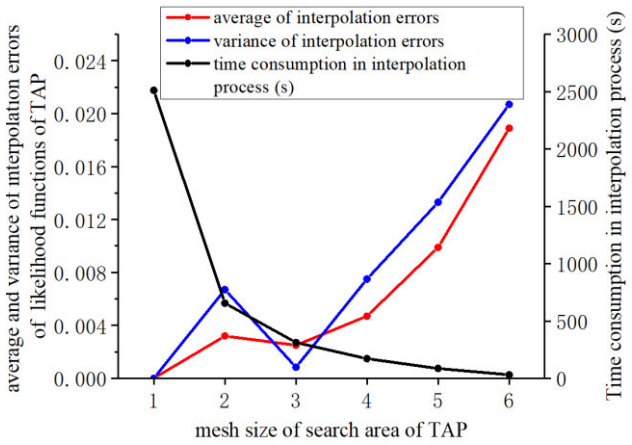

FIGURE 15. Time consumption and interpolation error with mesh refinement.

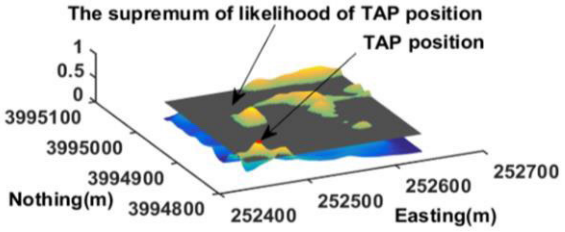

(a) Likelihood function and supremum plane of TAP position

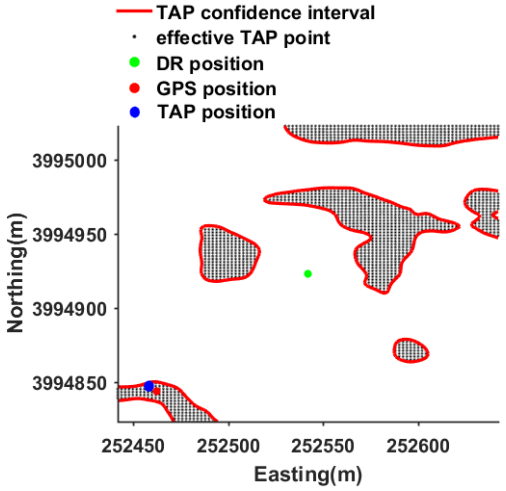

(b) The confidence interval and effective TAP position

FIGURE 16. A example of the calculation of the TAP confidence interval and effective TAP position.

step size but then increases rapidly. The interpolation error is on the order of 10^3 while the searching step is less than 4 m.

B. EFFICIENT TAP POSITION ESTIMATION AND PARTICLE INITIALIZATION

Equation (15) determines an isosurface, where the contour line obtained by intercepting the likelihood function at the isosurface is the confidence interval boundary of the TAP (Fig.16a and b). If the likelihood function value $L\left(\boldsymbol{X}^{kl}\right)$ of the search point $\boldsymbol{X}^{kl}$ $\left(\boldsymbol{X}^{kl} \in X^{s}\right)$ is greater than the lower bound $L_{1-\alpha}$ or equal to $L_{1-\alpha}$, then the searching point $\boldsymbol{X}^{kl}$ is the effective TAP point and is marked as $\boldsymbol{X}_{ij}^{c}$, and the point $\boldsymbol{X}_{ij}^{c}$ is included in the confidence interval $\boldsymbol{X}^{c}$ $\left(\boldsymbol{X}_{ij}^{c} \in X^{c}\right)$, $i = 1, 2, 3 \ldots C_{\mathrm{m}}, j = 1, 2, 3 \ldots C_{\mathrm{n}}$. C_{m} *and* C_{n} represent the row and column number of effective TAP points respectively,

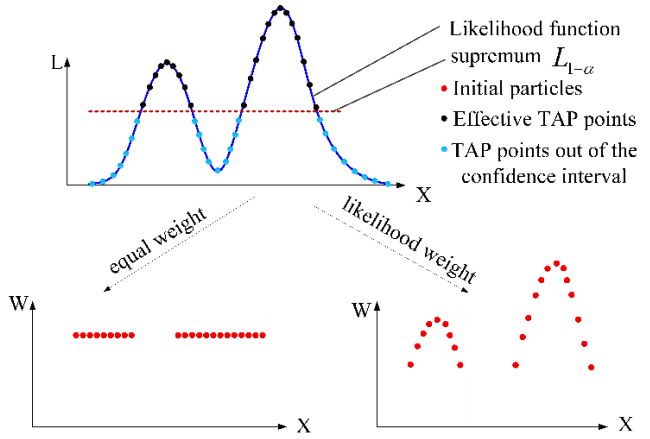

FIGURE 17. Arrangement of the same number of particles at the effective TAP point.

as shown in (19):

$$\begin{cases} if\ \left(L\left(\boldsymbol{X}_{ij}^{s}\right) > L_{1-\alpha}\right) \Rightarrow \boldsymbol{X}_{ij}^{s} \in \boldsymbol{X}_{ij}^{c} \\ \boldsymbol{X}_{ij}^{s} \in X^{s} \\ \boldsymbol{X}_{ij}^{c} \in X^{c} \end{cases} \tag{19}$$

where $L\left(\boldsymbol{X}^{kl}\right)$ represents the likelihood function value at search point $\boldsymbol{X}^{kl}$, X^{c} represents the confidence interval for TAP; $\boldsymbol{X}_{ij}^{c}$ represents the confidence interval point in X^{c}, and $L_{1-\alpha}$ represents the lowest bound of the likelihood function calculated by Equation (15). The schematic diagram of the search interval X^{s}, the search point $\boldsymbol{X}^{kl}$ $\left(\boldsymbol{X}^{kl} \in X^{s}\right)$) the confidence interval X^{c}, and the jump point $\boldsymbol{X}_{ij}^{c}$ $\left(\boldsymbol{X}_{ij}^{c} \in X^{c}\right)$ are described in Fig.16b.

The initialization of particles mainly considers the particle arrangement at $\left(\boldsymbol{X}_{ij}^{c} \in X^{c}\right)$. The same number of particles is arranged at each effective point; in the experiment, all the effective TAP positions distribute one particle. The question is how to define the initial weight of the initial particles. There are two methods:

1) Use the likelihood value of the effective TAP position as the initial weight, as shown in Fig.17. The likelihood function value of the effective TAP position reflects the probability of the AUV at this point; thus, it is reasonable to use the likelihood function value as the weight of the initial particles.

2) Give all initial particles equal weights, as shown in Fig.17, due to the possible existence of pseudo-positioning in terrain-matched positioning points. As the peak of the likelihood does not necessarily appear at the true position, the value of the likelihood at the true position is often smaller than the value of the likelihood at the TAP position when the positioning deviation occurs. Using equal weights can weaken the effect of the location deviation.

V. CONTRAST EXPERIMENT OF PARTICLE INITIALIZATION

DEM were obtained in 2010 by using a GS+ sounding sonar, and the main parameters are shown in **Table 1**. The data acquisition area is located in the Gulf of Jiaozhou, near the Zhong Sha reef (Fig.18). Topographic sounding equipment and their connections are shown in Fig. 11.

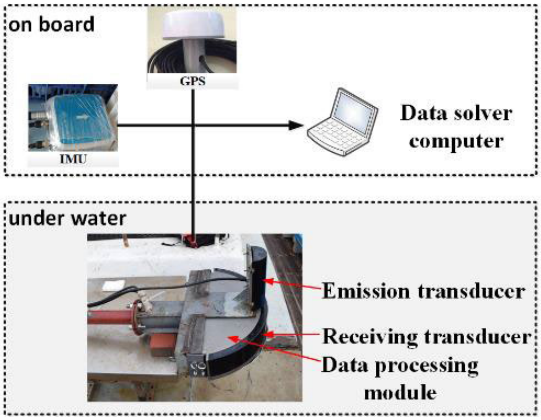

FIGURE 18. Real-time multi-beam measuring equipment.

TABLE 1. DEM parameters.

Area of DEM	891 m × 922 m
Resolution	1 m × 1 m
Average Depth	−16.5148 m
Maximum Depth	−6.03 m
Minimum Depth	−31.00 m
Origin of DEM	(251,931 m, 3,994,405 m)

TABLE 2. TAN Sensor parameters.

Multi-beam Sonar T-SEA CMBS200
Beam number /ping : 192 beams
Horizontal field angle: ≥ 140°
Horizontal beam width: ≤ 1°
Vertical beam width: ≤ 2°
Detection distance: ≥ 300 m
StarNeto XW-GI5651 INS/ GNSS: RTK of 20 cm (CEP)

MTM is measured using real-time multibeam sonar that can acquire terrain profile data in real time and realize online filtering terrain reconstruction. The sensor parameters are listed in **Table 2**.

The experiment uses playback simulation in order to test the algorithm; the raw data obtained from the real-time multi-beam measurement are used as input data. Due to the input error of the dead reckoning navigation system, and the dead reckoning navigation process is an integral process, the positioning error of the navigation system will increase with time, and eventually gradually deviate from the actual value more and more [9], [23]. Since the deviation of the DR position is approximately $5\% - 6\%$ of distance traveled (DT), the deviation of the DR position is up to 128 m in the initial TAN, and the initial search interval is an area 200m × 200m.

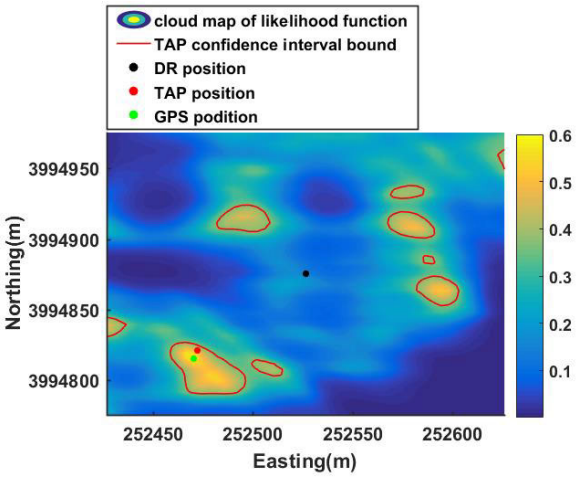

FIGURE 19. Cloud map of the likelihood function and the TAP confidence interval at the initial waypoint of TAN.

A. COMPARISON OF TWO INITIAL WEIGHT ASSIGNMENT METHODS

Fig.19 shows the cloud map of the likelihood function of an initial TAP, the confidence interval of the initial TAP, and the effective TAP position. As we can see, multiple pseudo-peaks appear in the likelihood function, and the confidence interval of initial TAP is scattered in the search area. However, the area of the confidence interval is far smaller than the search area.

Test1. Initialize the particle with likelihood weights

At first, estimate the confidence interval of TAP by using the method mentioned in **Section II**. Then, using the likelihood value as the initial weight of the initial particle as described in Fig.17 of **Section III**. The particle distribution at the initial waypoint and last waypoint are shown in Fig.20a. At the initial time of TAN, the location of AUV may exist in the black dots in the red rectangle in Fig.20a. After the TAN, these particles converge near the green points as show in Fig.20a. At the initial waypoint, the particles are concentrated in the TAP confidence interval as shown in Fig.20b, however, it eventually converges to the exact location (Fig.20a). The TAN track is shown in Fig.20b, and it converges to the GPS track and maintains high tracking accuracy. The TAN deviation is shown in Fig.20c. As we can see, the positioning deviation decreases rapidly in the initial phase and finally converges to the exact position.

Test2. Initialize the particle with equal weight

At first, estimate the confidence interval of TAP by using the method mentioned in **Section II**. Then, using the equal weight as the initial particle weight as described in Fig.17 of **Section III**. Fig.21a shows the PF results when the initial particle is assigned equal weight, and the particle eventually converges to the exact location. At the initial time of TAN, the location of AUV may exist in the black dots in the red rectangle in Fig.20a. After the TAN, these particles converge near the green points as show in Fig.20a. The TAN track is shown in Fig.21b, and TAN track converges to the GPS

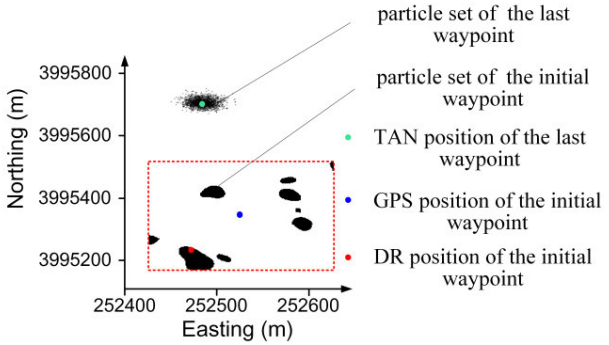

(a) Particle distribution of initial and last waypoint

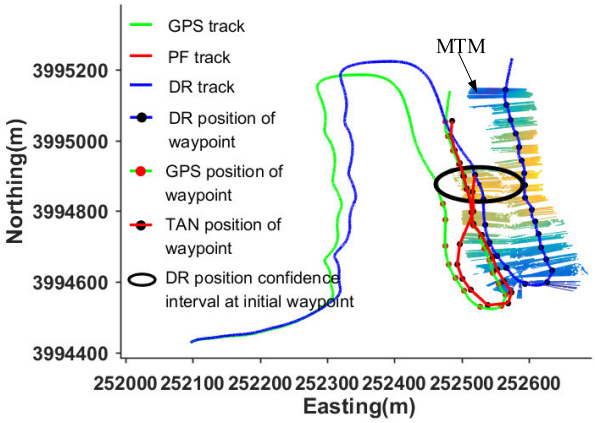

(b) TAN track and the MTM

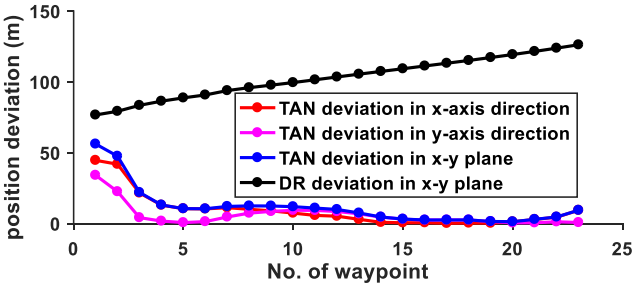

(c) Position deviation

FIGURE 20. Particle arrangement at effective TAP positions and initialize particles with likelihood weights.

track and maintains high tracking accuracy. The deviation of the PF is shown in Fig.21c, and the positioning deviation decreases rapidly after the filtering starts. The result is not much different from that of **Test1**.

B. COMPARISON WITH OTHER INITIALIZATION SCHEMES

Different initialization methods are used to initialize the particles at the initial TAN stage of TAN, and their filtering performance is subsequently compared. Next, we initialize the particles according to the other two initialization methods mentioned. One is the particle-filter initialization, which is based on reference navigation information (**Test3**), and the other is the particle initialization based on the search interval (**Test4**).

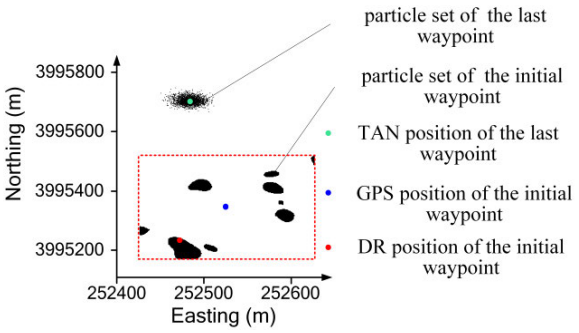

(a) Particle distribution of initial and last waypoint

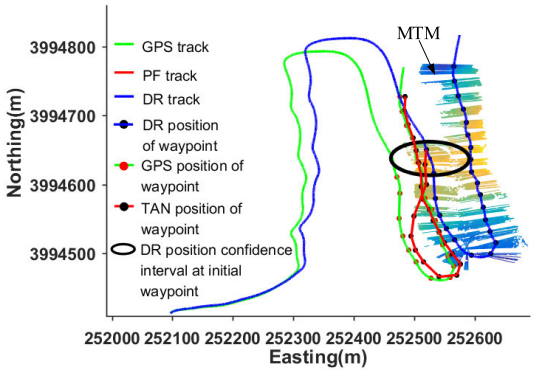

(b) TAN track and the MTM

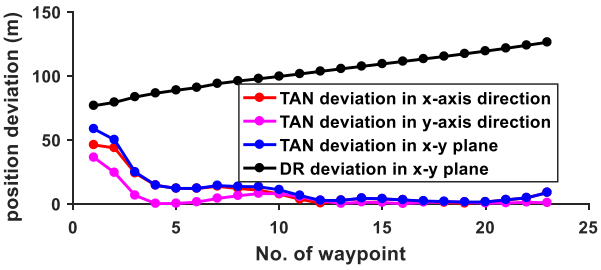

(c) Position deviation

FIGURE 21. **Arrangement particles at effective TAP positions and initialization of particles with equal weights.**

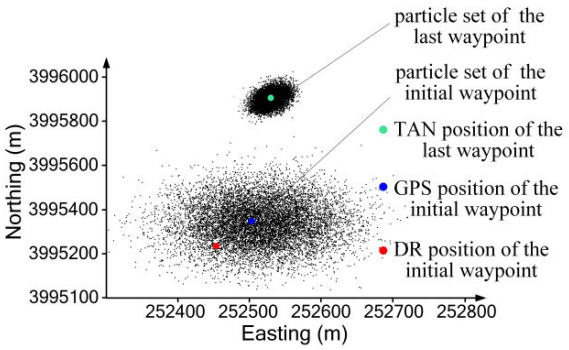

(a) Particle distribution of the initial and last waypoint

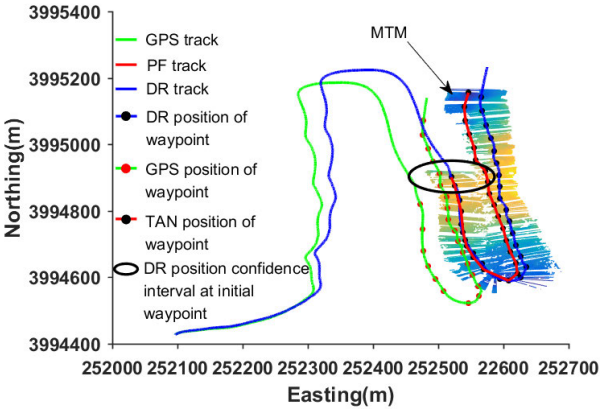

(b) TAN track and the MTM

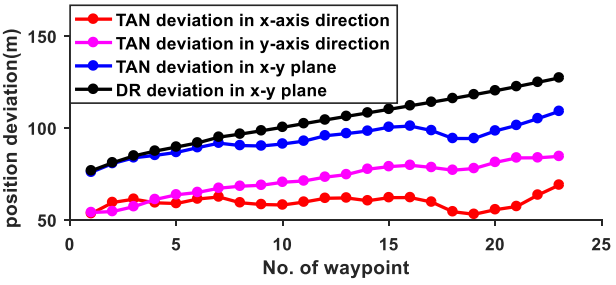

(c) Position deviation

FIGURE 22. **Initialization particles with DR position information.**

Test3. Initializing the particles based on DR information

Fig.22a shows the distribution of particles at the initial position that the obey Gaussian distribution with variance $\boldsymbol{P}_0$. At the initial time of TAN, the location of AUV may exist in the black dots set in the middle and lower part of fig.20a. After the TAN, these particles converge to the green point as show in Fig.20. The particles converge at the last TAN waypoint, but as shown in Fig.22b, the PF result is converged to the wrong position. The main reason is that the initial error and coverage range of initialization particles are too large, which results in the particles tracking the wrong terrain features. As shown in Fig.22c, the TAN position deviation has been increasing. This shows that TAN has completely diverged and the system is completely 'kidnapped' by the incorrect topographic features.

Test4. Particle initialization based on TAP searching area

The rectangle search interval computing method, and the search length:

$$\begin{cases} l_x = 2\gamma\sqrt{\mathrm{K}\lambda_1\cos^2(\theta) + \mathrm{K}\lambda_2\sin^2(\theta)} \\ l_y = 2\gamma\sqrt{\mathrm{K}\lambda_1\sin^2(\theta) + \mathrm{K}\lambda_2\cos^2(\theta)} \end{cases} \tag{20}$$

where, l_x and l_y representation in the x and y direction, respectively. K is a quantity related to confidence ε with $\varepsilon = 0.03$, λ_1, λ_2, θ defined in Equation (17), γ denotes the square amplification factor of the search interval, and K can be calculated by Equation (21).

$$\varepsilon = \frac{1}{\sqrt{2\pi}\det(\boldsymbol{P}_0)}\exp\left(\frac{\mathrm{K}}{2}\right) \tag{21}$$

TABLE 3. Statistics and comparisons of experimental results.

	A(m)	B (m)	C (m)	D (m)	E
Test1	11.81	19.94	4.35	8.65	2281
Test2	11.72	20.91	3.28	8.32	2281
Test3	93.47	87.01	99.38	109.04	10000
Test4	37.73	48.60	27.76	26.50	10000

This initialization method ignores the DR positioning information at the initial TAN time and considers the probability of each point $\boldsymbol{P}_{ij}$ in the search interval, obtained by the estimated navigation error, is equal to Equation (22). The initializing particles covered the entire search range (red rectangle area) that indicates the possible location of AUV, and the convergence of the particle at the last waypoint is not strong (Fig.23a). As show in Fig.23b, there is a big deviation between TAN track and GPS track. As shown in Fig.23c, PF converges slowly and its positioning accuracy is significantly improved compared to that of the DR initialization method (Fig.23c). The TAN position will be more accurate then **TEST3** while PF is initialized by search interval.

$$\boldsymbol{P}_{ij} = \frac{1}{\mathrm{m} \times \mathrm{n}} \tag{22}$$

The statistics and comparisons of **Test1**, **Test2**, **Test3**, and **Test4** are shown in **Table 3**. The four statistics are listed as follows:

A. The mean TAP point position deviates at all waypoints.
B. The mean TAP point position deviates in the convergence phase. The convergence phase refers to the TAP points from the first to the eleventh waypoint;
C. The mean TAP point position deviates in the tracking phase. The tracking phase refers to the TAP points from the twelfth to the last waypoint;
D. Positioning accuracy of terrain matching navigation endpoint.
E. The total number of particles obtained after the initialization.

It can be seen clearly from **Table 3** that when the DR deviation is very large at the initial TAN phase, the PF results, which were obtained using the DR information to initialize the particles, is very poor (**Test3**). Improved PF results can be obtained by the initialization of particles based on the TAP search area. However, the initial particles need to be arranged in a wide range, which increases the probability of similar terrain and makes the filtering convergence too slow (**Test4**). If an effective TAP point is obtained from the search point and initialized to the particle, the PF convergence rate will be faster. The TAN positioning accuracy at the last waypoint is obviously improved, and better results can be achieved using fewer particles (**Test1** and **Test2**).

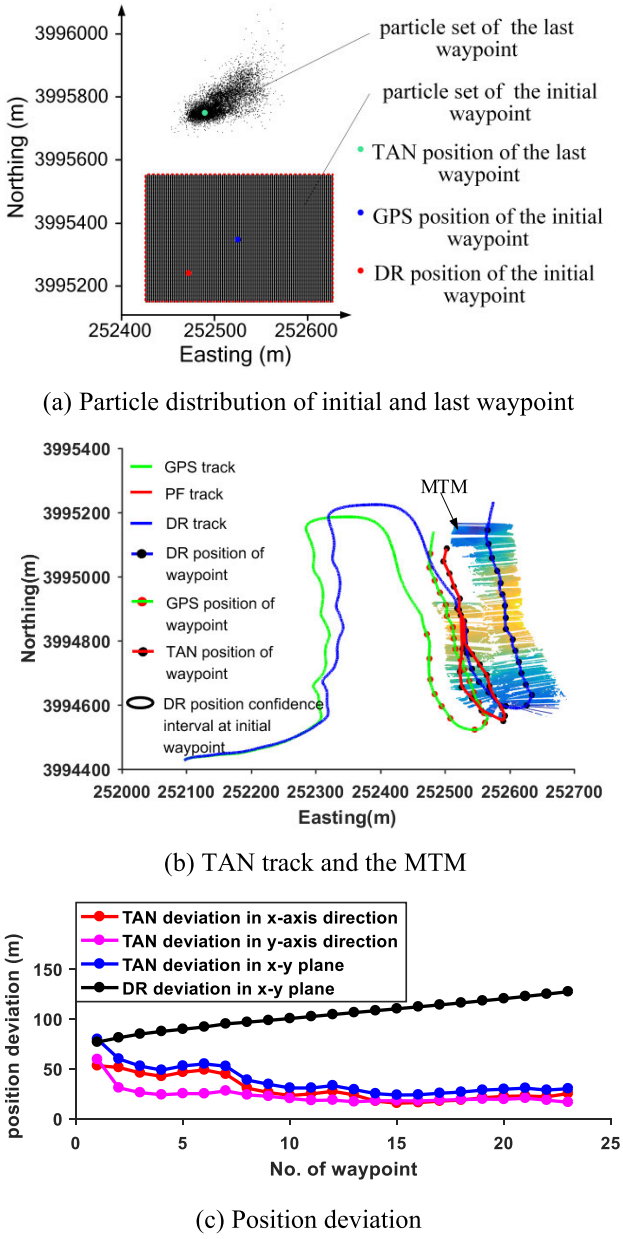

FIGURE 23. Arrangement particles in searching area and initialization with weight.

VI. CONCLUSION

The cumulative DR error will be very large when the AUV cannot receive position correction information for long periods of time, and the accumulated DR deviation reaches hundreds of meters in the initial phase. Thus, the initial particle coverage will be very large and cause the filtering convergence process to be very unstable. The filtering results fail to converge rapidly in the area with abundant topographic features, and diverge rapidly once entering the flat terrain. This seriously affects the stability and practicality of the TAN system, as the underwater vehicle cannot be accurately guided to the seabed target point. We propose estimating the TAP

confidence interval using the mathematical characteristics of the terrain surface and matching the TAP residuals, which is simpler and more practical than estimating it using the sensor error coupling relationship in a bathymetric system. The TAP confidence interval can constrain the initial position in a very small area and speed the convergence of PF. TAN filtering can converge to a stable value in a relatively short distance, thus improving the stability and accuracy of TAN system.

REFERENCES

[1] O. K. Hagen, K. B. Ånonsen, T. O. Sæbø, "Toward autonomous mapping with AUVs-Line-to-line terrain navigation," in *Proc. IEEE OCEANS*, Oct. 2015.

[2] G. M. Reis, M. Fitzpatrick, J. Anderson, J. Kelly, L. Bobadilla, and R. N. Smith, "Increasing persistent navigation capabilities for underwater vehicles with augmented terrain-based navigation," in *Proc. OCEANS*, Aberdeen, U.K., 2017, pp. 1–8.

[3] G. M. Reis, M. Fitzpatrick, J. Anderson, L. Bobadilla, and R. N. Smith, "Augmented terrain-based navigation to enable persistent autonomy for underwater vehicles," in *Proc. 1st IEEE Int. Conf. Robot. Comput. (IRC)*, Apr. 2017.

[4] J. Anderson and R. N. Smith, "Predicting water properties with Markov random fields for augmented terrain-based navigation in autonomous underwater vehicles," in *Proc. IEEE OCEANS*, Kobe, Japan, May 2018, pp. 1–5.

[5] G. Salavasidis, C. Harris, S. Mcphail, A. B. Phillips, and E. Rogers, "Terrain aided navigation for long range AUV operations at arctic latitudes," in *Proc. IEEE/OES Auto. Underwater Vehicles (AUV)*, Nov. 2016, pp. 115–123.

[6] G. Salavasidis, A. Munafò, C. A. Harris, T. Prampart, R. Templeton, M. Smart, D. T. Roper, M. Pebody, S. D. McPhail, E. Rogers, and A. B. Phillips, "Terrain-aided navigation for long-endurance and deep-rated autonomous underwater vehicles," *J. Field Robot.*, vol. 36, pp. 447–474, Mar. 2018.

[7] I. Nygren, "Terrain navigation for underwater vehicles," Ph.D. dissertation, Signal Process. Lab., Dept. Signals, Sensors Syst., School Elect. Eng., Roy. Inst. Technol., Stockholm, Sweden, 2005.

[8] K. B. Anonsen and O. Hallingstad, "Terrain aided underwater navigation using point mass and particle filters," in *Proc. IEEE/ION Position, Location, Navigat. Symp.*, Coronado, CA, USA, Apr. 2006, pp. 1027–1035.

[9] D. K. Meduna, *Terrain Relative Navigation for Sensor-Limited Systems With Application to Underwater Vehicles*. Stanford, CA, USA: Stanford Univ., 2011.

[10] S. M. Rock, B. Hobson, and S. E. Houts, "Return-to-site of an AUV using terrain-relative navigation: Field trials," in *Proc. IEEE/OES Auton. Underwater Vehicles*, Oct. 2014, pp. 1–8.

[11] F. C. Teixeira, J. Quintas, P. Maurya, and A. Pascoal, "Robust particle filter formulations with application to terrain-aided navigation: Robust particle filters for terrain-aided navigation," *Int. J. Adapt. Control Signal Process.*, vol. 45, no. 4, pp. 132–139, 2016.

[12] A. Murangira, C. Musso, K. Dahia, and J.-M. Allard, "Robust regularized particle filter for terrain navigation," in *Proc. 14th Int. Conf. Inf. Fusion*, Chicago, IL, USA, Jul. 2011, pp. 1–8.

[13] S. Dektor and S. Rock, "Improving robustness of terrain-relative navigation for AUVs in regions with flat terrain," in *Proc. IEEE/OES Auton. Underwater Vehicles (AUV)*, Southampton, U.K., Sep. 2012, pp. 1–7.

[14] Y.-G. Park and C. G. Park, "Grid support adaptation for point mass filter based terrain referenced navigation using mutual information," *IEEE Sensors J.*, vol. 18, no. 18, pp. 7603–7610, Sep. 2018.

[15] Y. M. Yoo and C. G. Park, "Improvement of terrain referenced navigation using a point mass filter with grid adaptation," *Int. J. Control Automat. Syst.*, vol. 13, no. 5, pp. 1173–1181, Oct. 2015.

[16] L. Paull, S. Saeedi, M. Seto, and H. Li, "AUV navigation and localization: A review," *IEEE J. Ocean. Eng.*, vol. 39, no. 1, pp. 131–149, Jan. 2014.

[17] P. Chen, Y. Li, Y. Su, X. Chen, and Y. Jiang, "Review of AUV underwater terrain matching navigation," *J. Navigat.*, vol. 68, no. 6, pp. 1155–1172, Nov. 2015.

[18] J. Melo and A. Matos, "Survey on advances on terrain based navigation for autonomous underwater vehicles," *Ocean Eng.*, vol. 139, pp. 250–264, Jul. 2017.

[19] L. Zhao, N. Gao, B. Huang, Q. Wang, and J. Zhou, "A novel terrain-aided navigation algorithm combined with the TERCOM algorithm and particle filter," *IEEE Sensors J.*, vol. 15, no. 2, pp. 1124–1131, Feb. 2015.

[20] F. C. Teixeira, J. Quintas, and A. Pascoal, "Robust methods of magnetic navigation of marine robotic vehicles," *IFAC-PapersOnLine*, vol. 50, no. 1, pp. 3470–3475, 2017.

[21] S. E. Houts, S. G. Dektor, and S. M. Rock, "A robust framework for failure detection and recovery for terrain-relative navigation," in *Proc. Unmanned Untethered Submersible Technol.*, Portsmouth, U.K., 2013.

[22] Y. Xie, "Terrain aided navigation," M.S. thesis, Project Signal Process. Lab., Dept. Signals, Sensors Syst., School Elect. Eng., Roy. Inst. Technol., Stockholm, Sweden, May 2005.

[23] G. Box, "Time series analysis: Forecasting and control," in *A Very British Affair* (Palgrave Advanced Texts in Econometrics). London, U.K.: Palgrave Macmillan, 2013.

[24] L. Zhou, X. Cheng, Y. Zhu, C. Dai, and J. Fu, "An effective terrain aided navigation for low-cost autonomous underwater vehicles," *Sensors*, vol. 17, no. 4, p. 680, Mar. 2017.

WANG RUPENG received the bachelor's degree in naval architecture and ocean engineering from Chongqing Jiaotong University, in 2013, and the master's degree from the Science and Technology on Underwater Vehicles Laboratory, Harbin Engineering University, in 2015, where he is currently pursuing the Ph.D. degree (without examination). He is also a Postdoctoral Researcher with Hohai University. His research directions are underwater guidance, integrated navigation, and underwater detection.

LI YE received the bachelor's degree (Eng.) in shipping and marine engineering from Harbin Engineering University, in 2001, the master's degree from the Science and Technology on Underwater Vehicles Laboratory, Harbin Engineering University, in 2005, and the Ph.D. degree in 2007. He is the Deputy Director of the Science and Technology on Underwater Vehicles Laboratory, Harbin Engineering University. His main research direction is navigation and control of autonomous underwater vehicle.

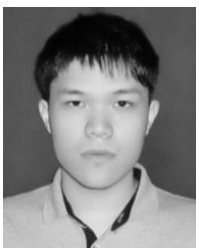

MA TENG received the bachelor's degree in shipping and marine engineering from Harbin Engineering University, in 2015, where he is currently pursuing the Ph.D. degree with the Science and Technology on Underwater Vehicles Laboratory. His main research direction is underwater SLAM.

CONG ZHENG received the bachelor's degree in shipping and marine engineering from Harbin Engineering University, in 2016, and the master's degree from the Science and Technology on Underwater Vehicles Laboratory, Harbin Engineering University, 2018, where he is currently pursuing the Ph.D. degree. His research direction is underwater SLAM.

GONG YUSEN received the bachelor's degree in shipping and marine engineering from Harbin Engineering University, in 2016, where he is currently pursuing the Ph.D. degree with the Science and Technology on Underwater Vehicles Laboratory. His main research direction is underwater SLAM.

XU PENGFEI received the bachelor's and master's degrees from Harbin Engineering University, in 2002 and 2005, respectively, and the Ph.D. degree in ship and marine structure design and manufacture from the China Ship Science Research Center, in March 2014. He currently holds a postdoctoral position in ship and marine engineering with Shanghai Jiao Tong University, and the Institute of Marine Equipment and Underwater Technology, Hohai University, where he is also the Director of the Institute.